IV. AXIAL SOLIDS DISTRIBUTION

Knowledge of axial solids distribution is essential to properly design a slurry bubble column reactor. The distribution of solid particles in a bubble column reactor has an effect on reactant conversion and may affect product selectivity (Bukur and Kumar, 1986; Smith and Ruether, 1985). Operating conditions (i.e. gas and slurry velocity), physical properties of the liquid medium, particle size and density, and column diameter influence the axial distribution of solid particles in a slurry bubble column reactor.

In this study, the effect of particle size and type, column diameter, slurry velocity and gas velocity on axial solids distribution was examined. The semi–infinite dispersion model presented by Smith and Ruether (1985) was used to analyze our results. The theory (semi–infinite dispersion model), a summary of the average solids concentrations in the bubble column and storage tank during each run, and results (i.e. axial solids distributions and axial solids dispersion coefficients) from our studies are discussed.

Semi–Infinite Dispersion Model

Several variations of the one–dimensional sedimentation dispersion model, based on different frames of reference, are available in the literature. The model presented by Parulekar and Shah (1980) is based on the cross–sectional area of the column; whereas, the models by Cova (1966), Kato et al. (1972), Smith and Ruether (1985), and O'Dowd et al. (1987), are based on the cross–sectional area occupied by the slurry phase alone (i.e. the area associated with the gas phase is not included). More recently, Murray and Fan (1989) developed a mechanistic model to describe the solids distribution in slurry bubble columns. In the present analysis, the model presented by Smith and Ruether (1985) was used to analyze our experimental data. Their one–dimensional dispersion

model is given by

$$\frac{\delta}{\delta x}\left[\frac{-E_s}{h_{exp}}\frac{\delta C_s}{\delta x}\right]+\frac{\delta}{\delta x}\left[\left[\frac{u_{s\ell}}{(1-\epsilon_g)}-\Phi_\ell u_p\right]C_s\right]=h_{exp}\frac{\delta c_s}{\delta t} \tag{4.1}$$

where x is the dimensionless height above the distributor (based on the expanded height, h_{exp}), E_s is the axial solids dispersion coefficient, C_s is the solids concentration in the slurry, $u_{s\ell}$ is the average slurry flow rate, u_p is the hindered settling velocity of the solid particles, Φ_ℓ is the volume fraction of liquid in the slurry, and t is the time. The solids concentration in the slurry, C_s is defined as

$$C_s=\omega_s\rho_{s\ell} \tag{4.2}$$

where ω_s is the weight fraction of solids and $\rho_{s\ell}$ is the density of the slurry.

Since the volume fraction of liquid in the slurry, Φ_ℓ, does not vary significantly with axial position (less than 3% for our experiments), an average value may be used and is defined as:

$$\overline{\Phi_\ell}=(1-\frac{\overline{C_s}}{\rho_s}) \tag{4.3}$$

where ρ_s is the density of the solids and $\overline{C_s}$ is the average solids concentration in the slurry and is given by

$$\overline{C_s}=\frac{\sum_i C_{s_{ij}}V_{ij}}{V_T} \qquad i=1 \text{ to } 5 \text{ and } j=i+1 \tag{4.4}$$

where V_T is the total volume of slurry, V_{ij} is the volume of slurry between pressure ports i and j (see Figure 2.9) and $C_{s_{ij}}$ is the solids concentration in the slurry between pressure ports i and j. Note, j = 6 corresponds to the top of the column. The total volume of slurry is

$$V_T=h_{exp}(1-\epsilon_g) \tag{4.5}$$

where h_{exp} is the expanded height of the dispersion and ϵ_g is the average gas holdup in the column. The volume of slurry between pressure ports i and j is

$$V_{ij} = \Delta h_{ij}(1 - \epsilon_{g_{ij}}) \qquad i = 1 \text{ to } 5 \text{ and } j = i + 1 \tag{4.6}$$

where Δh_{ij} is the distance between pressure ports i and j and $\epsilon_{g_{ij}}$ is the axial gas holdup in the i,j section of the column.

For batch experiments (i.e. $u_{s\ell} = 0$) at steady state (no time derivatives), and assuming no dependency of Φ_ℓ on height, Eq. 4.1 reduces to

$$\frac{\delta}{\delta x}\left[\frac{-E_s}{h_{exp}}\frac{\delta C_s}{\delta x}\right] - \frac{\delta}{\delta x}\left[\overline{\Phi_\ell} u_p C_s\right] = 0 \tag{4.7}$$

Equation 4.7 may be integrated twice to yield:

$$C_s = C_1 + C_2 \exp\left[-h_{exp}\overline{\Phi_\ell}\frac{u_p}{E_s}x\right] \tag{4.8}$$

For the semi–infinite dispersion model, the boundary conditions are given by: $C_s = 0$ as x approaches infinity and $C_s = C_s^B$ for x=0, where C_s^B is the concentration of solids at the bottom of the dispersion. Application of these boundary conditions to Eq. 4.8 yields:

$$C_s = C_s^B \exp\left[-h_{exp}\overline{\Phi_\ell}\frac{u_p}{E_s}x\right] \tag{4.9}$$

Solids concentration vs. axial position data can now be used to obtain estimates of $\frac{u_p}{E_s}$ and the concentration of solids at the bottom of the column, C_s^B, using regression analysis.

For continuous slurry flow, the solution to Eq. 4.1 is:

$$C_s = (C_s^B + a)\exp\left[-(u_p\overline{\Phi_\ell} - u'_{s\ell})\frac{h_{exp}}{E_s}x\right] - a \tag{4.10}$$

where $a = \frac{u'_{s\ell} C_s^f}{\Phi_\ell u_p - u_{s\ell}}$ and $u'_{s\ell} = \frac{u_{s\ell}}{(1-\epsilon_g)}$. The quantity C_s^f is the concentration of solids in the feed (or storage tank). It is assumed that no settling occurs in the feed stream (i.e.,

at $x<0$, $u_p = 0.0$ and $\frac{\delta C_s}{\delta x} = 0.0$). In developing Eqs. 4.9 and 4.10, it was assumed that the gas holdup did not vary with axial position. The assumption of an axially uniform gas holdup holdup profile leads to the assumptions of a constant (i.e. no axial variation) dispersion coefficient and a constant hindered settling velocity. With the exception of experiments in which foam was produced, axial gas holdup profiles were fairly uniform (see Figures 2.14 and 2.15). The model also assumes a uniform particle size.

A variety of approaches may be used to obtain values for u_p, E_s, and C_s^B (see Eq. 4.10). Kato et al. (1972) assumed that E_s and u_p were not affected by slurry velocity, $u_{s\ell}$. They used the quantity $\frac{u_p h_{exp}}{E_s}$ obtained from batch experiments (see Eq. 4.9) together with two points taken from a smoothed plot of concentration versus axial position (continuous experiment) to obtain a value for $\frac{u'_{s\ell} h_{exp}}{E_s}$, from which E_s was calculated. Then substituting the values of E_s and h_{exp} into $\frac{u_p h_{exp}}{E_s}$, a value for u_p was obtained. On the other hand, Smith and Ruether (1985), used non–linear regression analysis of Eq. 4.10 to obtain E_s, u_p, and C_s^B.

For batch experiments, u_p and E_s are not separable, and in order to obtain axial dispersion coefficients, one must assume values for the hindered settling velocity of the solids, u_p. There are various correlations available in the literature for estimating the hindered settling velocity (e.g. Kato et al., 1972; Smith and Ruether, 1985; Zigrand and Sylvester, 1980; and O'Dowd et al., 1987). The correlations proposed by Kato et al., Smith and Ruether, and O'Dowd et al. are all of the form

$$u_p = a u_t^b u_g^c \overline{\Phi_\ell}^d \tag{4.11}$$

where u_t is the terminal rise velocity of a single particle in an infinite medium. The numerical values of constants (a, b, c, and d) in Eq. 4.10 are (1.33, 0.75, 0.25, 2.5) for Kato et al., (1.91, 0.8, 0.26, 3.5) for Smith and Ruether, and (1.69, 0.8, 0.23, 1.28) for O'Dowd et al. correlation.

Several correlations have been presented in the literature for predicting axial dispersion coefficients. The correlation proposed by Kato et al. is:

$$Pe_p = \frac{13Fr_g(1 + 0.009Re_pFr_g^{-0.8})}{1 + 8Fr_g^{0.85}} \tag{4.12}$$

The equation presented by Smith and Ruether is:

$$Pe_p = 9.6\left[\frac{Fr_g^6}{Re_g}\right]^{0.114} + 0.019Re_p^{1.1} \tag{4.13}$$

and the equation presented by O'Dowd et al. for an unbaffled bubble column is:

$$Pe_p = 7.7\left[\frac{Fr_g^6}{Re_g}\right]^{0.098} + 0.019Re_p^{1.1} \tag{4.14}$$

where $Pe_p = \frac{u_g d_{col}}{E_s}$, $Re_g = \frac{u_g d_{col}\rho_\ell}{\mu_\ell}$, $Fr_g = \frac{u_g}{\sqrt{g d_{col}}}$, and $Re_p = \frac{d_p \rho_\ell u_t}{\mu_\ell}$. The terms containing Re_p in Eqs. 4.12 to 4.14 are correction factors which take into account particle size. Due to insufficient data with different size particles, O'Dowd et al., used the correction factor presented by Smith and Ruether. Murray and Fan (1989) also presented an empirical correlation for predicting axial solids dispersion coefficients, E_s; however, their correlation does not take into account the effect of column diameter.

Summary of Solids Concentrations in the Column and Storage Tank

As mentioned in Chapter II, slurry samples were withdrawn from the storage tank and column during three–phase experiments. Table 4.1 contains the nominal solids concentration for each run, as well as the range of average solids concentration in the column and in the storage tank during each run. Also shown in Table 4.1 is the total amount of solids charged in the storage tank and the total amount of solids accounted for during each experiment. The experiment numbers given in the first column of Tables

4.1a (0.05 m ID column) and 4.1b (0.21 m ID column) correspond to the experiment numbers given in Tables 2.4 and 2.5, respectively.

For experiments conducted with small particles, the solids concentrations measured in both the storage tank and column were usually within 3 % (absolute) of the desired (or nominal) concentration. However, very low solids concentrations were observed in both the storage tank and bubble column during our initial continuous experiments with large iron oxide particles (experiments 19 and 20 in Table 4.1a) in the 0.05 m ID column. Following these experiments, the entire system was inspected and approximately 50% of the initial amount of solids charged in the storage tank was recovered in the expansion unit. The expansion unit was modified to reduce the amount of settling (see Figure 4.1). Partitions were added inside the expansion unit to minimize the surface area available for the deposition of solids. Experiments 26 and 27 were conducted with large iron oxide particles at superficial slurry velocities of 0.02 and 0.005 m/s following the modification of the expansion unit. There was some settling of solids during these experiments; however, the amount of settling was substantially less than that previously observed (i.e. the solids concentration in the column was 18 – 19 %). During experiment 27 ($u_{s\ell}$ = 0.005 m/s), the overflow line from the expansion unit to the calibration chamber (see Figure 4.1) plugged during the last gas velocity (i.e. u_g = 0.02 m/s), and the solids concentration in column dropped considerably (i.e. ω_s (column) = 19.2% at u_g = 0.04 m/s and 9.3 % at u_g = 0.02 m/s). Also, during this same experiment solids concentrations in the storage tank were very low (i.e. 6.9 – 8.4 wt%). Similar results were obtained during the experiment with SASOL wax and large iron oxide particles at a slurry flow rate of 0.005 m/s (see results for experiment 33 in Table 4.1a).

Solids accountability (large particles) was substantially better for experiments conducted in the large diameter column, with the exception of experiments 15 and 16 (see Table 4.1b). The solids concentration in these two experiments (both in the column and

Table 4.1a. Summary of Solids Concentrations for Experiments in the 0.05 m ID Bubble Column

EXP. No.	u_f (m/s)	SOLIDS[a]	NOMINAL CONC (WT %)	AVG CONC IN COLUMN (WT %)	AVG CONC IN TANK (WT %)	AMOUNT CHARGED (g)	AMOUNT ACCOUNTED TANK+COLUMN (g)
4	0.005	1	10	9.5–10.0	N/A	1900	N/A
5	0.02	1	10	8.9–9.5	N/A	1900	N/A
6	0.0	1	10	9.5–10.2	N/A	1900	N/A
7	0.005	1	20	16.4–17.4	15.8–17.4	3910	3000–3100
8	0.02	1	20	17.3–17.7	16.9–18.3	3910	3400–3600
9	0.0	1	20	18.5–19.1	19.4	3910	3200
10	0.005	1	30	28.4–28.9	27.9–29.3	7282	6220–6300
11	0.02	1	30	28.5–29.3	27.6–28.6	7282	6300–6500
12	0.0	1	30	29.2–29.6	28.5–29.1	7282	6325–6370
13[e]	0.005	2	10	3.0–5.0	3.0–5.0	1765	200–650
14	0.005	3	10	9.2–10.5	8.6–9.4	1766	1410–1580
15	0.005	3	20	18.9–20.0	18.8–19.2	4284	3600–3800
16	0.02	3	20	17.2–18.6	18.1–19.1	4284	3400–3700
17	0.0	3	20	18.0–20.0	17.68	4284	3300–3400
18	0.005	3	30	26.3–28.1	25.1–27.1	7926	5100–5500
19	0.005	2	10	2.5–3.6	1.2–1.7	1816	230–370
20	0.02	2	10	5.3–6.5	4.2–5.2	1816	680–840
21	0.0	2	20	21.4–24.0	21.2	4103	3871–3960
22	0.0	4	20	7.5–8.2,20.2[b]	18.3	2800	2741
25	0.0	2	20	10.16–17[c]	19.3	4540	4120
26	0.02	2	20	17.8–19.5	15.6–17.0	4540	3600–3730
27	0.005	2	20	9.21–22.6[d]	6.9–8.4	4540	1790–2710
28	0.0	4	20	17.8–18.7	19.4	3280	3050
31	0.005	1	20	17.0–21.3	17.2–18.2	3936	3180–3540
32	0.0	2	20	18.3–22.6	18.5	3973	3820
33	0.005	2	20	14.6–18.3	9.9–10.8	3973	2032–2086
34[e]	0.005	2	20	N/A	N/A	3973	N/A

[a] 1: 0 – 5 μm iron oxide
2: 20 – 44 μm iron oxide
3: 0 – 5 μm silica
4: 20 – 44 μm silica

[b] 20 wt% at u_g = 0.12 m/s

[c] 10 wt% at u_g = 0.02 m/s

[d] 9 wt% at u_g = 0.02 m/s

[e] Pump shut down during the experiment

Table 4.1b. Summary of Solids Concentration for Experiments in the 0.21 m ID Bubble Column

EXP. No.	u_ℓ (m/s)	SOLIDS[a]	NOMINAL CONC (WT %)	AVG CONC IN COLUMN (WT %)	AVG CONC IN TANK (WT %)	AMOUNT CHARGED (g)	AMOUNT ACCOUNTED TANK+COLUMN (g)
6	0.0	1	10	9.7–10.1	9.2	13620	13260
7	0.0	1	20	18.0–19.9	20.6	30418	30640
8	0.005	1	20	20.2–20.7	20.4–20.9	30418	28550–29940
9	0.02	1	20	20.2–21.2	20.9–21.2	30418	28400–30300
10	0.0	1	20	19.0–21.2	20.3	30418	29680
11	0.005	1	20	20.3–21.0	19.7–21.1	30418	28500–29140
12	0.0	1	20	20.4–22.1	19.5	30418	27310
13	0.0	1	30	29.0–30.7	28.7–29.9	47216	45800–44970
14	0.005	30	29.3–30.3	29.5–30.0	47216	39400–43400	
15[b]	0.005	2	10	6.4–8.5	7.1–7.5	14272	8210–10120
16[b]	0.02	2	10	0.6–7.7	2.2–8.6	14272	1900–5160
17	0.0	2	20	17.2–22.2	21.1	41016	41467
18	0.005	2	20	20.9–24.9	18.0–20.9	41016	34310–39770
19	0.02	2	20	22.7–23.7	20.7–22.4	41016	40410–41100
20	0.0	2	20	18.5–22.9	N/A	41016	N/A
21	0.0	2	20	14.9,23.0–24.6[c]	N/A	41016	N/A
22	0.0	2	30	36.5–37.4	29.4	68710	63823
23	0.005	2	30	34.1–35.1	30.5–32.1	68710	59750–69240
24	0.02	2	30	33.1–36.6	32.4–34.9	68710	59750–69240
26	0.0	4	20	23.7–26.7	23.8	37355	39400
27	0.005	4	20	19.0–20.1	19.9–21.6	37355	31900–34100
28	0.02	4	20	18.5–23.0	19.5–21.8	37355	31970–34400
29	0.005	4	30	33.6–35.4	33.4–34.0	60764	60890–62470
33	0.0	2	20	13.0[c],20.4–21.2	N/A	30645	N/A
34	0.005	2	20	17.2–20.7	13.7–17.4	30645	21550–27704
35	0.005	2	20	15.8[c],19.9–21.5	14.4,18.0–19.7	33709	25320–35650

[a] 1: 0 – 5 μm iron oxide
2: 20 – 44 μm iron oxide
4: 20 – 44 μm silica

[b] Poor solids suspension in the storage tank

[c] Low solids concentrations at u_g = 0.02 m/s was due to settling in the bottom of the column

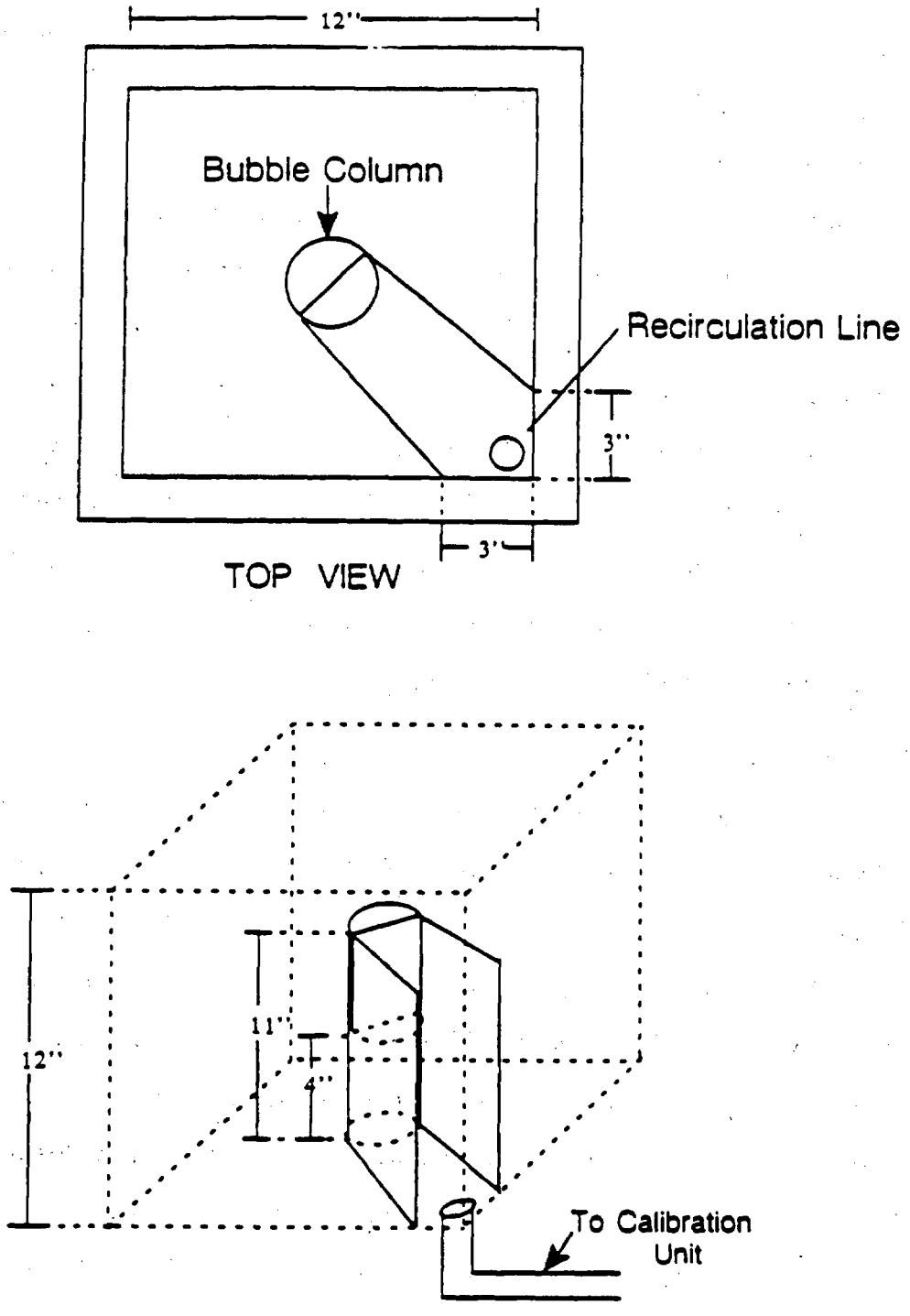

FIGURE 4.1. Schematic diagram of modified expansion unit.

storage tank) was considerably lower than the nominal wt% solids. After these runs, the system was shut down and inspected. It was found that the majority of solids had settled at the bottom of the storage tank. In order to improve mixing in the storage tank, a new propeller was installed. Following this modification, solids concentrations in the storage tank and bubble column were similar to the desired (or nominal) concentration. During three of the experiments with large particles (i.e. experiments 21, 33, and 35 in Table 4.1b), solids settled in the bottom of the column at a gas velocity of 0.02 m/s. Since we were unable to account for these solids, the measured solids concentrations in both the bubble column and storage tank were low at this gas velocity.

Following each batch of experiments, the slurry (wax + solids) was removed from the system and weighed. For experiments in the small column, approximately 90 – 95% of the slurry charged was recovered. And, for experiments in the large column, approximately 95 – 99% of the slurry charged was recovered.

Results and Discussion

Solids concentration profiles obtained from batch experiments in the 0.05 m ID column with large (i.e. 20 – 44 μm) iron oxide and silica particles were analyzed using the one–dimensional sedimentation dispersion model to obtain axial solids dispersion coefficients, E_s. Due to operational problems with both the pump (i.e. inability to maintain a constant flow rate) and settling of solids in the expansion unit, solids concentration data from experiments conducted in the continuous mode of operation in the small column were not analyzed. Data from both batch and continuous (one) experiments in the 0.21 m ID column with large particles were analyzed to obtain axial solids dispersion coefficients.

Regardless of the slurry flow rate, particle type, or column diameter, axial solids distributions were fairly uniform at all gas velocities for experiments conducted with

small (i.e. 0 – 5 μm) particles. Figures 4.2a and 4.2b show axial solids concentrations (wt%) from batch experiments conducted with slurries containing 20 wt% small iron oxide and small silica particles, respectively, in the 0.05 m ID column. The decrease in axial solids concentration at a height of 2.2 m is due to the inability of the foam to suspend the solids. Solids concentrations from a batch experiment with 0 – 5 μm iron oxide particles (20 wt%) in the 0.21 m ID column are shown in Figure 4.2c. Axial solids concentrations for experiments with small particles varied by less than 2 wt% (actual) across the entire column during all continuous experiments.

Solids concentration profiles from batch experiments with 20 wt% 20 – 44 μm iron oxide and silica particles in the 0.05 m ID column are shown in Figures 4.3a and 4.3b, respectively. During these experiments, significant gradients in the axial solids distribution were observed. Our results from the continuous experiments with large iron oxide particles show that a slight upward slurry velocity (0.02 m/s) significantly improves the suspension of solids (see Figure 4.3c). During this experiment, there were some problems with the pump, and the actual slurry velocity ranged from approximately 0.01 to 0.03 m/s. However, these results indicate that solids suspension, which does not show any noticeable improvement when gas velocity is increased (see Figures 4.3a and 4.3b) improves significantly with the introduction of a small upward slurry flow. This is expected since the terminal settling velocity for large iron oxide particles is about 0.001 m/s and that for silica particles is 0.0004 m/s. Both of these values are well below the slurry circulation velocity (0.01 – 0.03 m/s).

Figures 4.4a and 4.4b show solid concentration profiles for batch experiments conducted with large iron oxide particles in the 0.21 m ID bubble column with the perforated plate (PP) and bubble cap (BC) distributors, respectively. Axial solids concentration profiles from experiments with the PP and BC distributors were similar. Solids concentration gradients in the small column for batch experiments with large particles (see

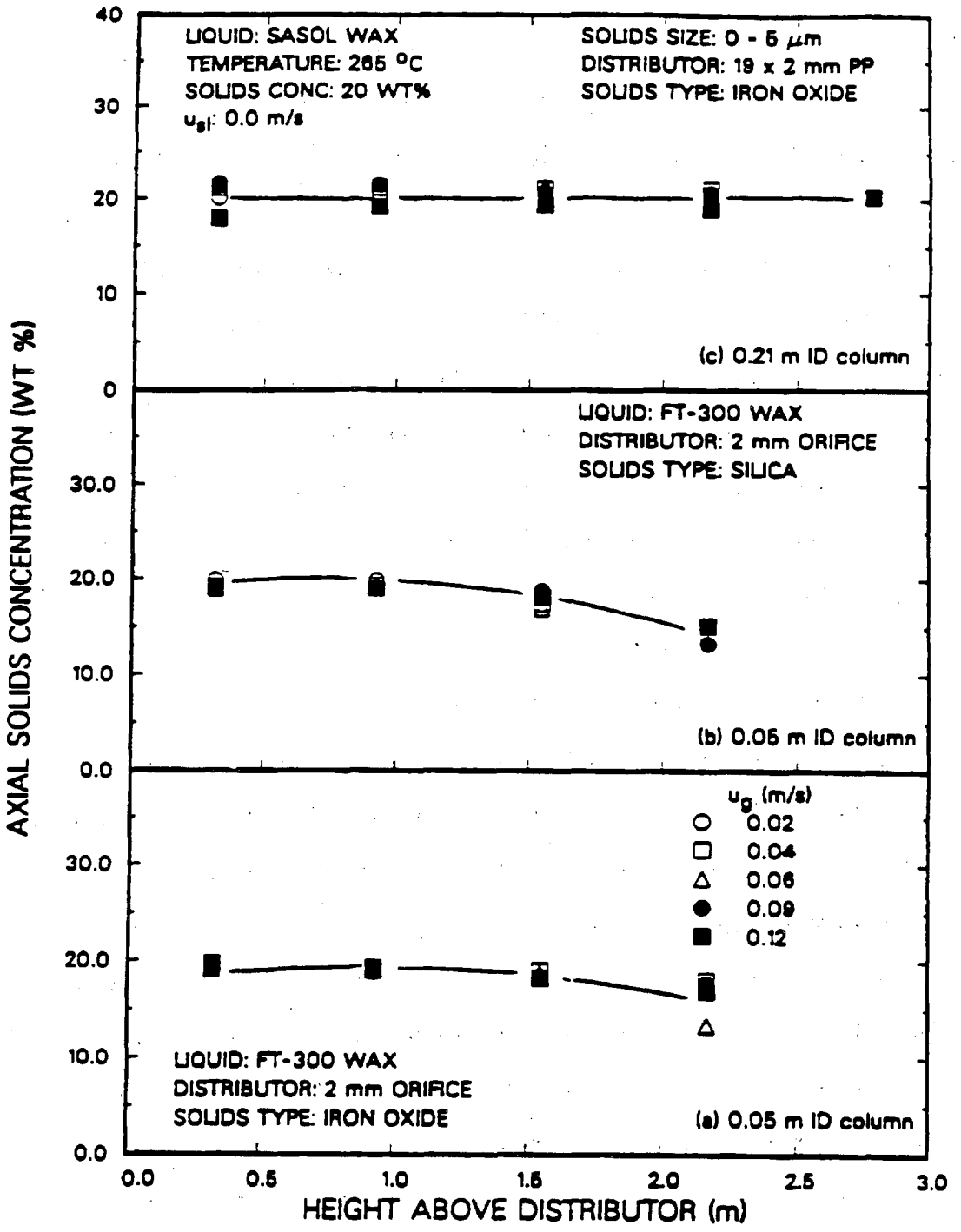

Figure 4.2. Effect of axial position and superficial gas velocity on solids concentrations (20 wt%, 0 - 6 μm particles, u_{sl} = 0.0 m/s; (a) iron oxide, 0.05 m ID column; (b) silica, 0.05 m ID column; (c) iron oxide, 0.21 m ID column).

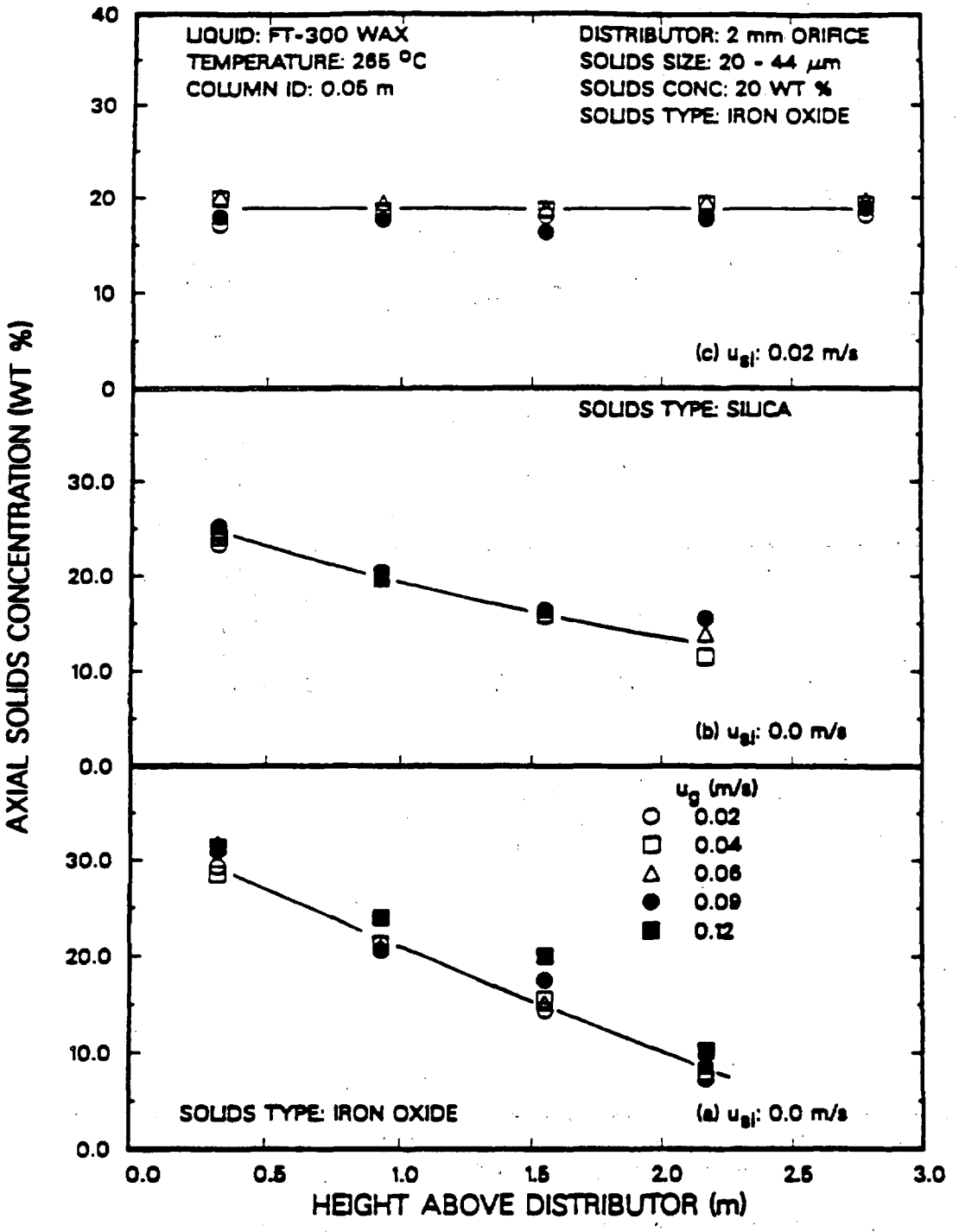

Figure 4.3. Effect of axial position and superficial gas velocity on solids concentrations (20 - 44 μm particles, 0.05 m ID bubble column; (a) iron oxide, u_{sl}=0 m/s; (b) silica, u_{sl}=0 m/s; (c) iron oxide, u_{sl}=0.02 m/s).

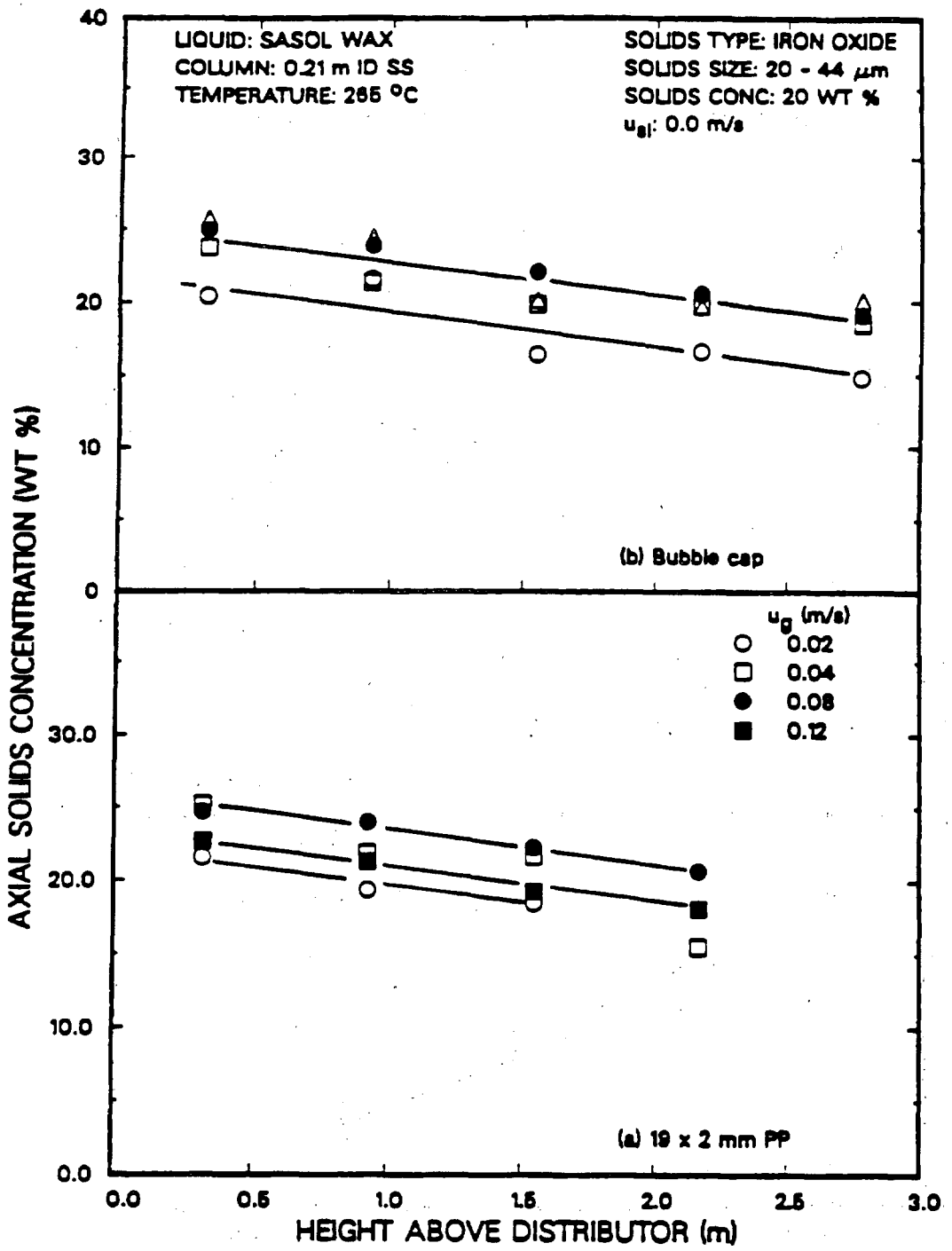

Figure 4.4. Effect of axial position and superficial gas velocity on solids concentrations (20 wt% 20 - 44 μm iron oxide particles, 0.21 m ID bubble column, u_{sl}=0 m/s; (a) 19 x 2 mm PP distributor; (b) bubble cap distributor).

Figures 4.3a and 4.3b) were steeper than those observed in the large column for experiments conducted in the batch mode of operation with large particles (see Figures 4.4a and 4.4b). This trend is expected since intense circulation patterns develop in the large diameter column which help to suspend the solid particles. A similar trend was observed with large silica particles in the 0.05 and 0.21 m ID columns.

Solids concentration profiles were fairly uniform for experiments conducted with both large iron oxide and large silica particles in the continuous mode of operation in the 0.21 m ID column. For experiments conducted with a slurry velocity of 0.02 m/s, the solids concentration profiles were essentially uniform (i.e. ω_s varied by less than 2 wt% (actual) across the entire column). During the experiment conducted with 30 wt% large iron oxide particles at a slurry velocity of 0.005 m/s, a slight solids concentration gradient was observed (see Figure 4.5a). Results from other experiments with large iron oxide particles at a superficial slurry velocity of 0.005 m/s also indicated a slight decrease in solids concentration with increase in height above the distributor; however, during these runs, the solids concentration profiles in the column below a height of 2.2 m fluctuated with axial position (see Figure 4.5b). Thus, the only data (i.e. axial solids concentrations) from a continuous experiment that were analyzed, were from the experiment conducted with 30 wt% large iron oxide particles at a slurry velocity of 0.005 m/s.

Axial solids dispersion coefficients for iron oxide and silica were estimated using solids distribution profiles from batch mode experiments in both the 0.05 m and 0.21 m ID bubble columns via Eq. 4.9. A total of three batch experiments with large iron oxide particles were conducted in the 0.05 m ID bubble column, two with FT–300 wax as the liquid medium and the other with SASOL wax as the liquid medium. Two batch mode experiments were also conducted in the small diameter column with large silica particles suspended in FT–300 wax. A total of four batch mode experiments with large

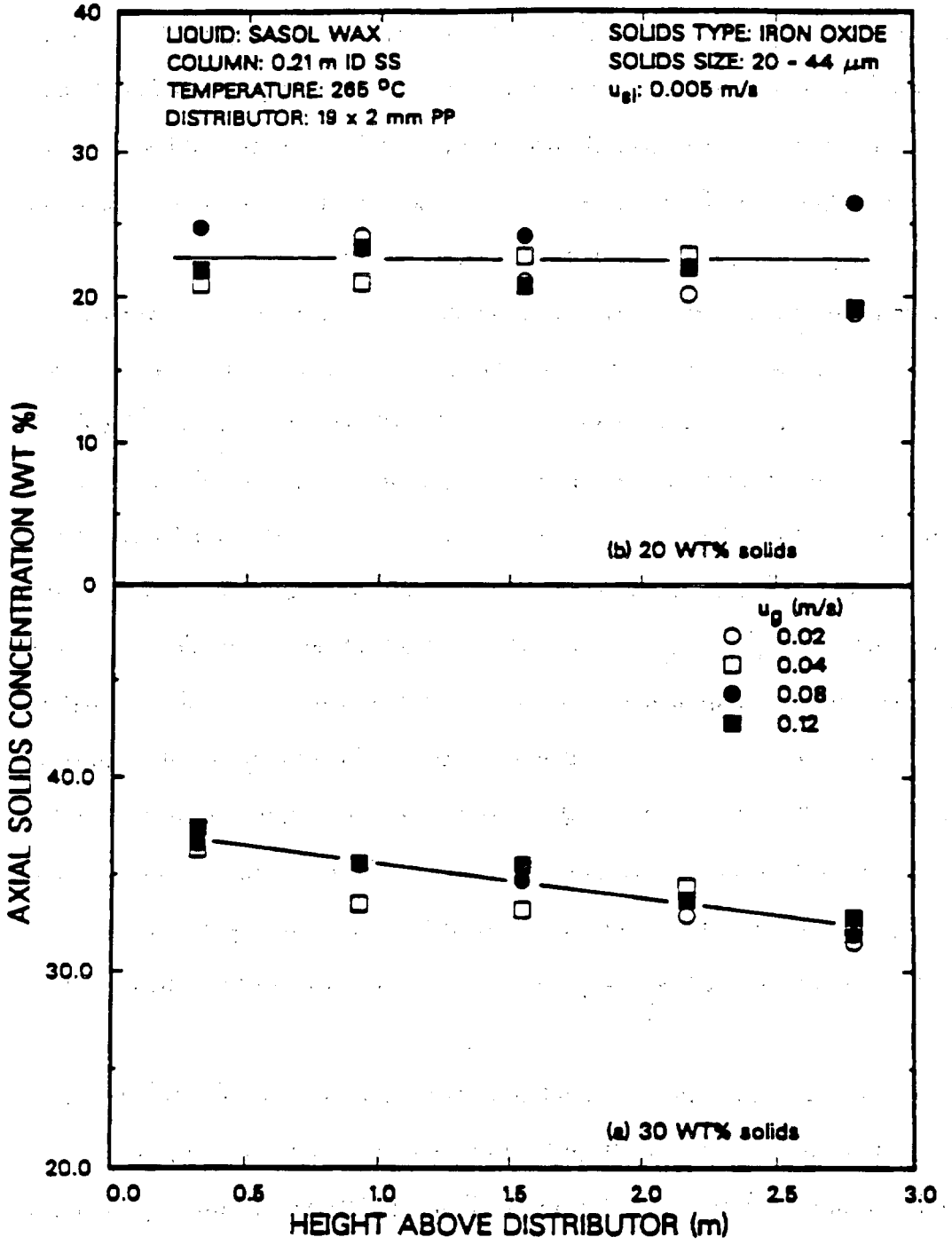

Figure 4.5. Effect of axial position and superficial gas velocity on solids concentrations (20 - 44 μm iron oxide particles, 0.21 m ID bubble column, u_{sl}=0.005 m/s; (a) 30 wt %; (b) 20 wt %).

iron oxide particles were conducted in the large diameter column, three with SASOL wax and the other with FT-300 wax as the liquid medium.

Figure 4.6 shows the effect of superficial gas velocity on the quotient $\frac{u_p}{E_s}$, which was estimated by fitting solids concentration (g/cc) vs. normalized axial height data to Eq. 4.9. Figures 4.6a and 4.6b correspond to values of $\frac{u_p}{E_s}$ obtained from batch experiments in the small diameter column with large iron oxide and large silica particles, respectively. Figure 4.6c shows results from batch experiments with large iron oxide particles in the 0.21 m ID column. Values of $\frac{u_p}{E_s}$ obtained from different experiments with large silica particles in the 0.05 m ID column were similar (Figure 4.6b); whereas, there was some variation in the values of $\frac{u_p}{E_s}$ obtained from different experiments with large iron oxide particles in the small column, particularly at a gas velocity of 0.02 m/s (Figure 4.6a). u_p / E_s values obtained from different experiments with large iron oxide particles in the large column were comparable (see Figure 4.6c).

As noted earlier, for batch mode experiments, the terms u_p and E_s are not separable, and hindered settling velocities must be assumed in order to estimate the dispersion coefficients. Hindered settling velocities and axial solids dispersion coefficients were obtained from the experiment conducted at a superficial slurry velocity of 0.005 m/s with 30 wt%, 20 – 44 μm iron oxide particles in the large diameter column using non-linear regression analysis (NLIN on SAS) of the experimental data (i.e. fit data (solids concentration vs. normalized height) to Eq. 4.10). The solids concentration of the feed, C_s^f, was assumed to be equal to the average solids concentration in the storage tank. The values of u_p from this experiment agreed with the values predicted using the correlation presented by Kato et al. (1972); whereas, the correlations presented by Smith and Ruether (1985) and O'Dowd et al. (1987) overestimated the hindered settling velocities (see Figure 4.7). Thus, the correlation presented by Kato et al. (Eq.

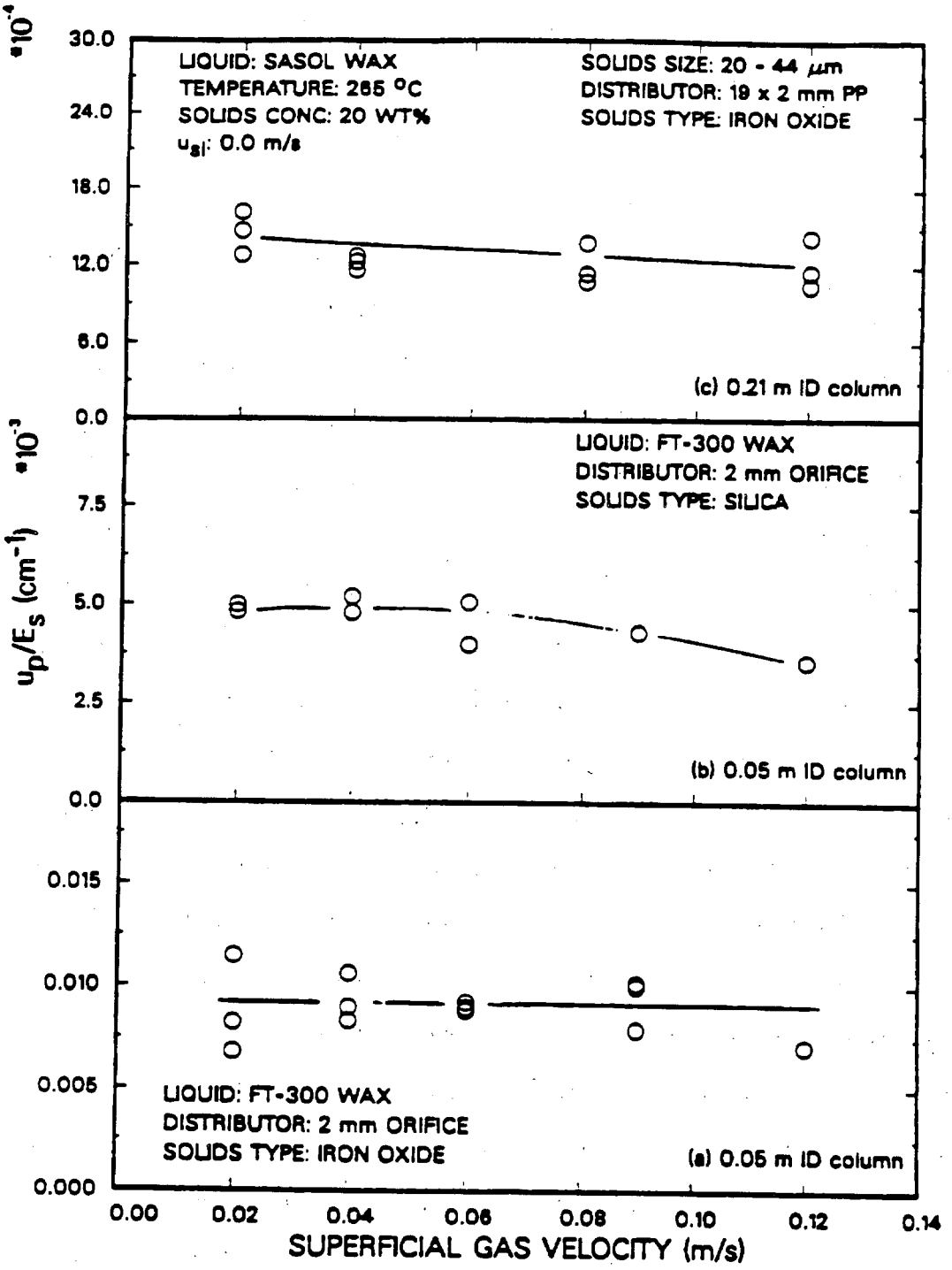

Figure 4.6. Effect of superficial gas velocity on u_p/E_s (20 - 44 μm particles, u_{sl} = 0.0 m/s; (a) iron oxide, 0.05 m ID column; (b) silica, 0.05 m ID column; (c) iron oxide, 0.21 m ID column).

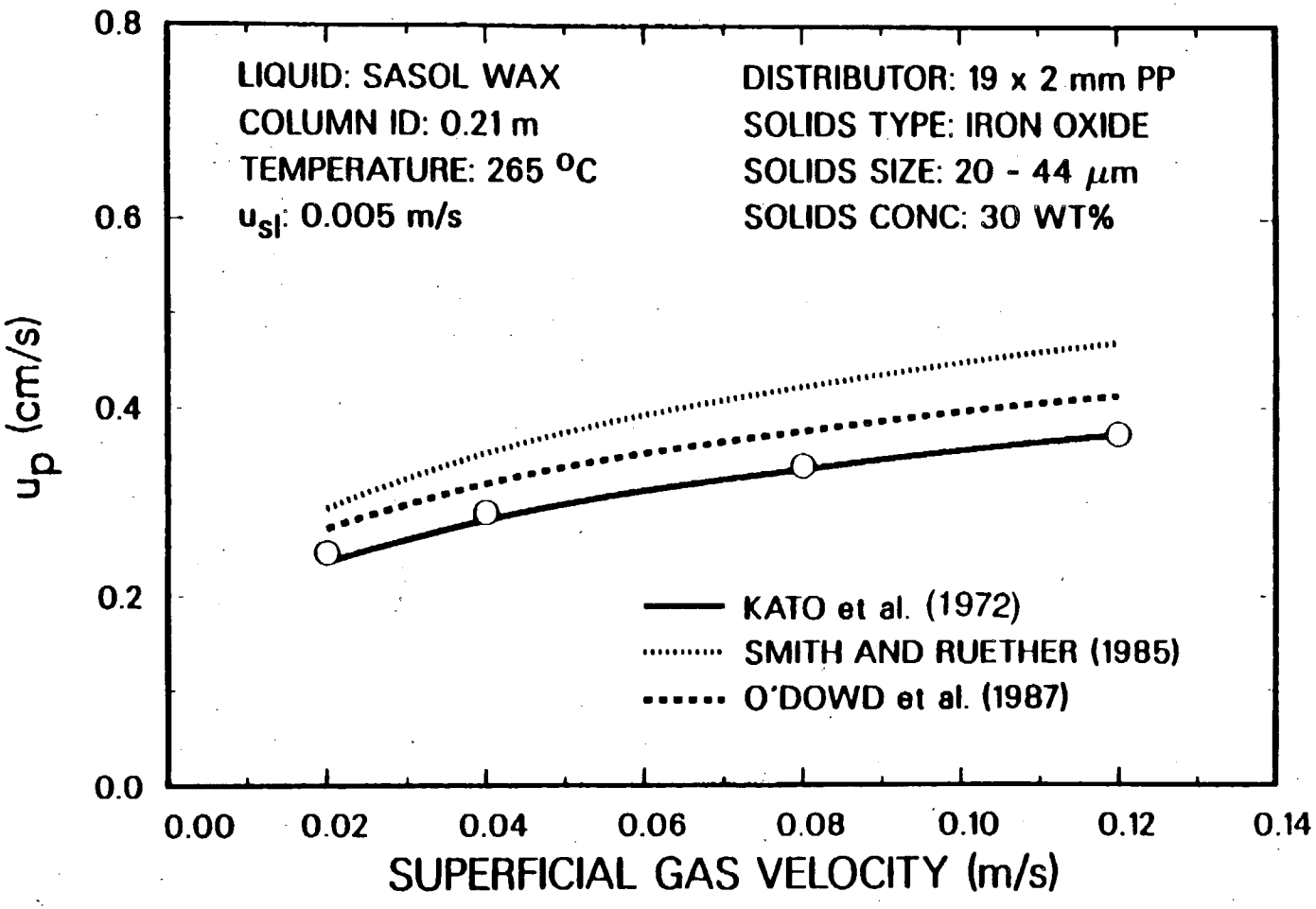

Figure 4.7. Effect of superficial gas velocity on hindered particle settling velocity for 20 - 44 μm iron oxide particles in SASOL reactor wax.

4.11) was used to calculate the hindered settling velocities needed to obtain the axial solids dispersion coefficients for experiments conducted in the batch mode of operation.

Axial solids dispersion coefficients, E_s, for batch experiments in both columns were calculated using $\frac{u_p}{E_s}$ (from least square fit of experimental data) and u_p (from Kato et al.'s correlation). The following correlation for the particle Pectlet number, Pe_p, which is similar to the ones presented by Smith and Ruether (1985) (Eq. 4.13) and O'Dowd et al. (1987) (Eq. 4.14) was developed

$$Pe_p = 8.4\left[\frac{Fr_g^6}{Re_g}\right]^{0.107} = \frac{u_g d_{col}}{E_s} \qquad (4.15)$$

for $0.014 < Fr_g < 0.271$ and $283 < Re_g < 7140$. The estimated parameters (i.e. 8.4 and 0.107) in Eq. 4.15 are comparable to those given by Smith and Ruether (9.6 and 0.114) and O'Dowd et al. (7.7 and 0.098).

Figures 4.8a and 4.8b show results for axial dispersion coefficients from experiments conducted with large particles in both the 0.05 m and 0.21 m ID columns, respectively, together with the predicted dispersion coefficients obtained using Eq. 4.15. The correlation overestimates the measured axial solids dispersion coefficients at gas velocities greater than 0.06 m/s in the large diameter column and underestimates the axial dispersion solids coefficients in the small diameter column at gas velocities less than 0.06 m/s. Axial solids dispersion coefficients obtained from the experiment in the large diameter column with the bubble cap distributor were consistently lower than those obtained from experiments with the perforated plate distributor at high gas velocities.

Figure 4.9 compares predicted and measured axial solids concentrations (g/cc). The predicted solids concentrations were obtained using Eq. 4.15 to predict the axial solids dispersion coefficient, E_s, and Kato et al.'s (1972) correlation to predict the hindered settling velocity, u_p. These quantities were then used in Eq. 4.9 to obtain the solids concentration at a given axial location for batch mode experiments. The solids

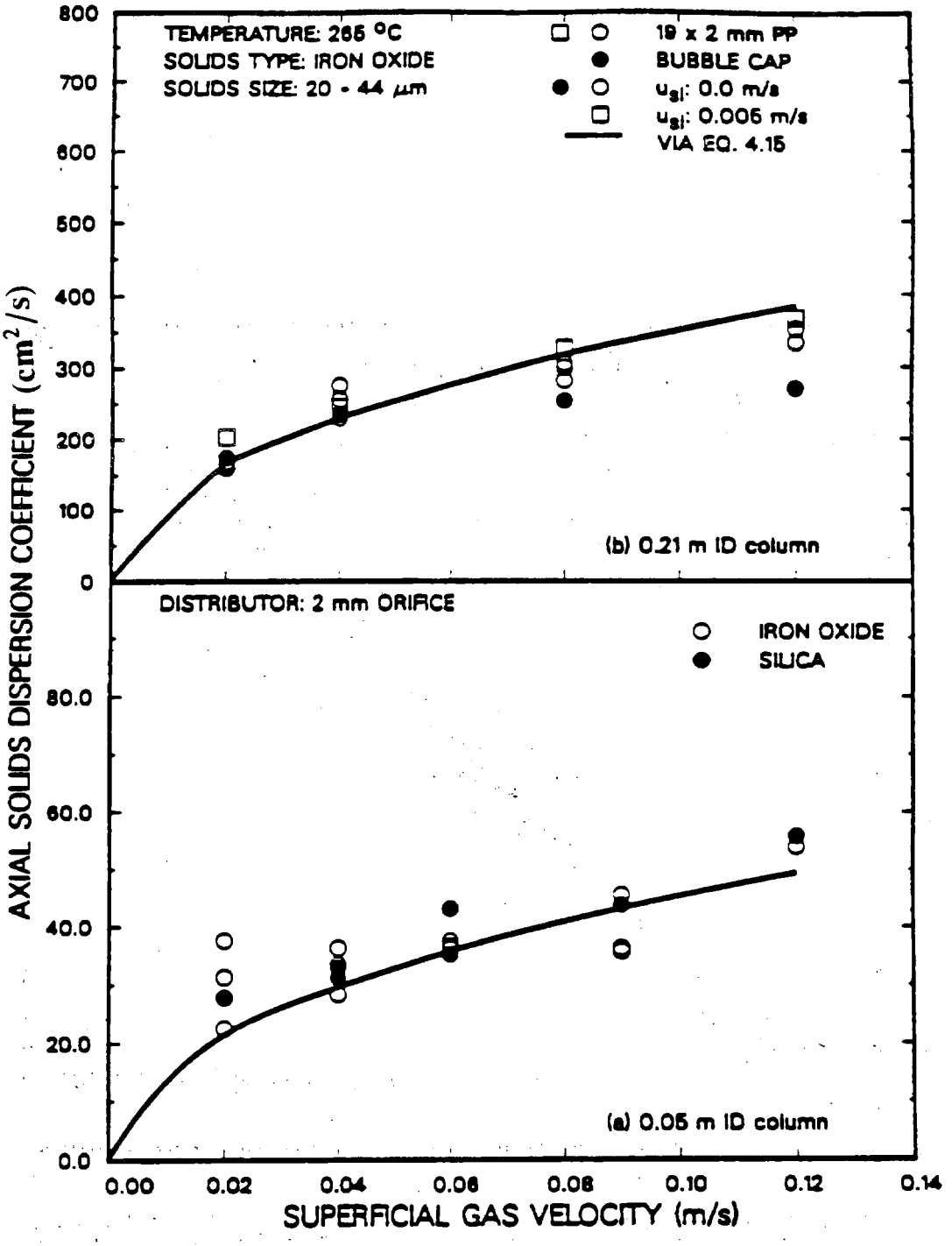

Figure 4.8. Effect of superficial gas velocity on axial solids dispersion coefficients ((a) 0.05 m ID column, (b) 0.21 m ID column).

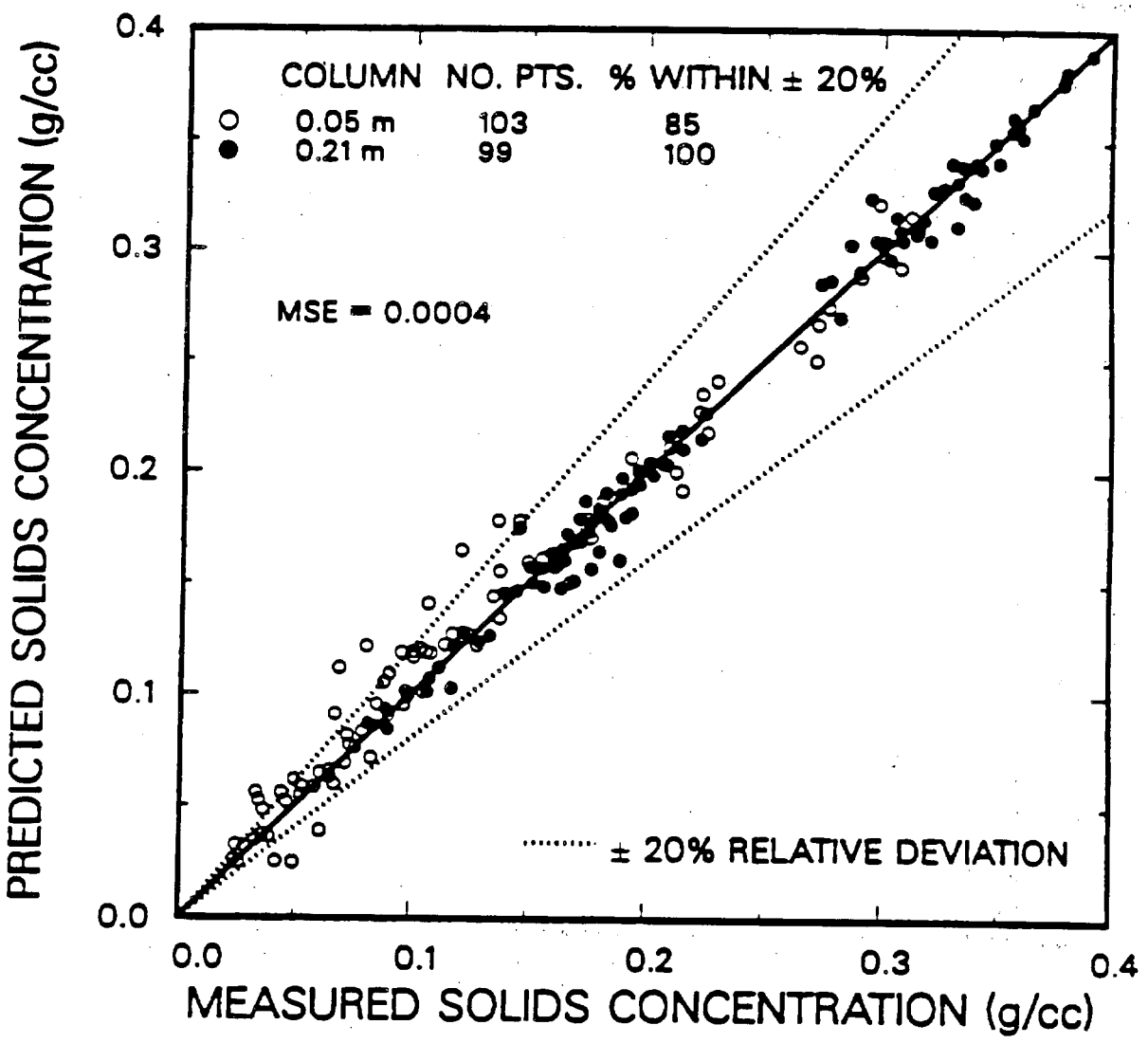

Figure 4.9. Parity plot of measured versus predicted solids concentrations; (20 - 44 μm iron oxide and silica particles; u_{sl} = 0.0 m/s and 0.005 m/s - 0.21 m ID column only).

concentration at the bottom of the column, C_s^B, was assumed to be the same as that obtained in the original analysis. For the experiment conducted in the continuous mode, the solids concentration profile was obtained using Eq. 4.10 with C_s^B and C_s^f being the same as determined in the original analysis. As shown in Figure 4.9 there is excellent agreement between the predicted and measured solids concentrations in both the small and large diameter columns.

As mentioned previously, no attempt was made to obtain axial solids dispersion coefficients for experiments conducted in the batch mode of operation with small particles because of the uniform solids concentration profiles. Theoretical solids concentration profiles for iron oxide and silica at gas velocities of 0.01, 0.12, and 0.30 m/s (Figures 4.10a and 4.10b, respectively) were determined. These profiles were obtained using the normalized (with respect to the solids concentration at the bottom of the column, C_s^B) form of Eq. 4.9. The axial solids dispersion coefficients were obtained from Eq. 4.15 and the hindered settling velocity were calculated from Eq. 4.11 using the constants given by Kato et al. (1972). The expanded height, h_{exp} was assumed to be 3 m. As shown in Figure 4.10, the solids concentration profiles for both iron oxide and silica are fairly uniform, and show very little effect of gas velocity. Similar trends were observed with our experimental data (see Figures 4.2a and 4.2b).

The effect of particle size (iron oxide) on the theoretical solids concentration distribution at gas velocities of 0.01, 0.12, and 0.30 m/s is shown in Figures 4.11a, 4.11b, and 4.11c, respectively. Particle sizes of 3 and 30 μm are representative of the average size of the particles used in the present study. The predicted trends (i.e. increasing solids concentration gradient with increasing particle size) are in agreement with those obtained from our experiments (symbols in Figure 4.11b). An increase in gas velocity decreases the concentration gradient along the height of the bubble column. However,

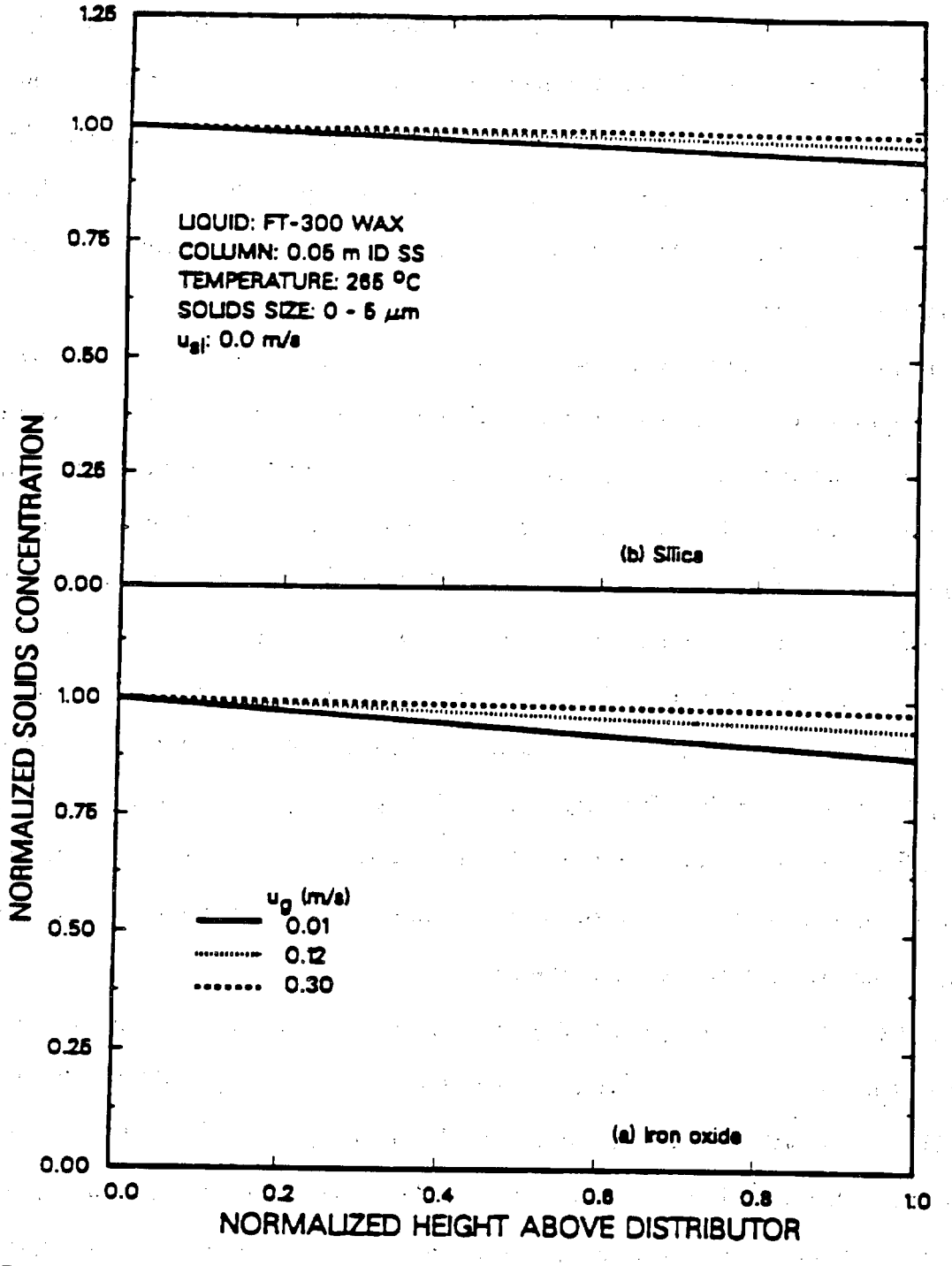

Figure 4.10. Effect of superficial gas velocity on axial solids concentrations (0 - 5 μm particles; 0.05 m ID bubble column; u_{sl}=0 m/s; (a) iron oxide (b) silica).

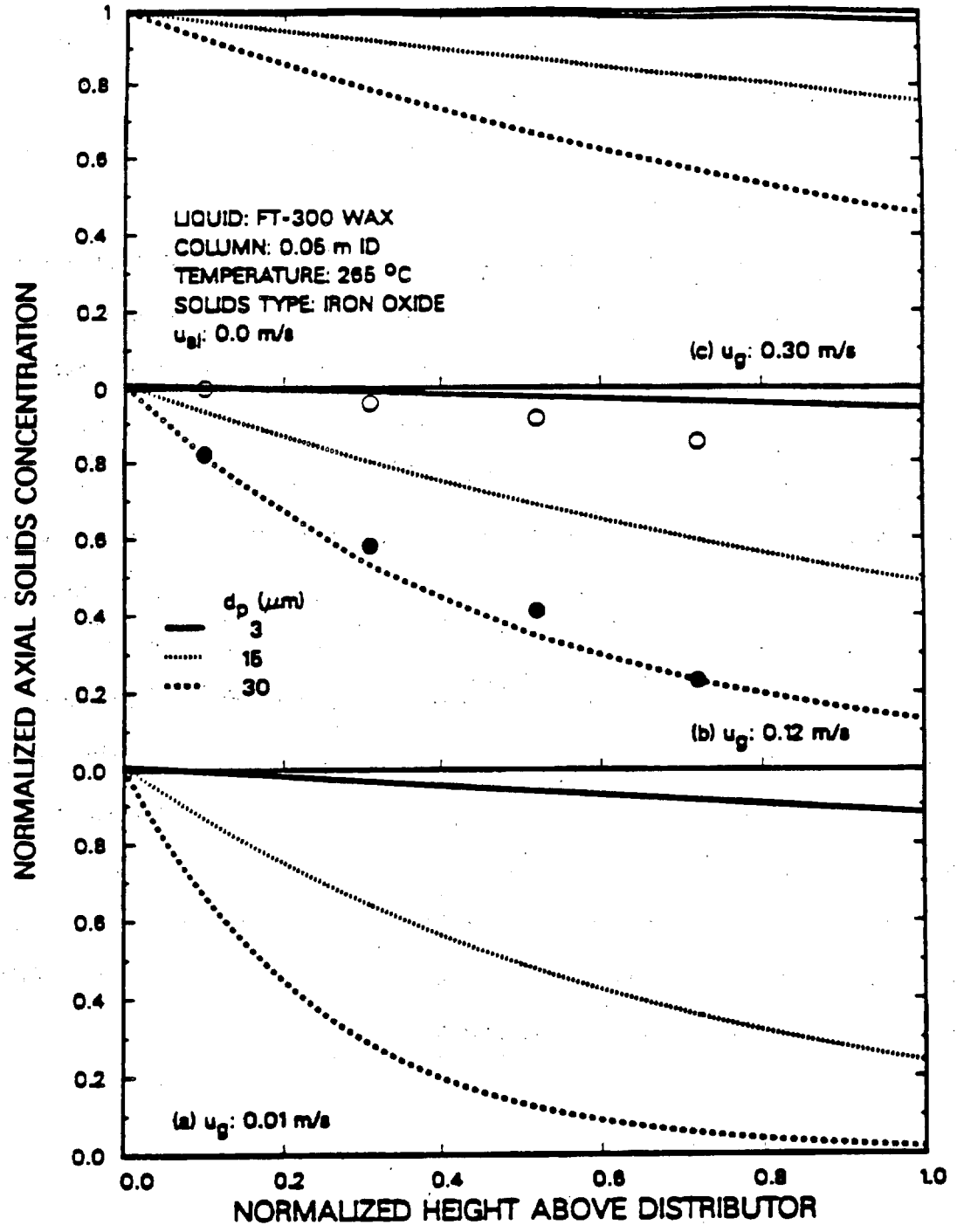

Figure 4.11 Effect of particle size and superficial gas velocity on axial solids concentrations.

(● - Experimental data with 20-44 μm particles;

○ - Experimental data with 0-5 μm particles)

even for a gas velocity of 0.30 m/s, there is still approximately a 58 % decrease in the solids concentration along the height of the reactor for 30 μm particles.

Figures 4.12a and 4.12b show the effect of slurry flow rate on solids (20 – 44 μm iron oxide particles) suspension in both the 0.05 and 0.21 m ID bubble columns, respectively. Also shown in Figure 4.12 are data obtained from batch experiments in the small and large diameter columns. The results presented in Figure 4.12 were obtained from Eq. 4.10, using Eq. 4.15 to estimate E_s and Eq. 4.11 to estimate u_p (Kato et al.'s constants). The solids concentrations were normalized with respect to the concentration at the bottom of the column, C_s^B. There is excellent agreement in the solids concentration obtained from the theory and those measured experimentally in both columns ($u_{s\ell} = 0$ m/s). At a slurry velocity of 0.02 m/s in the small column, the solids concentration profile is essentially uniform, which agrees with the results from our study (see Figure 4.3c). The theory predicts that a concentration gradient will exist in the small diameter column at a slurry velocity of 0.005 m/s with large iron oxide particles (see Figure 4.12a). However, due to operational problems with our pump, we were not able to obtain data at this slurry velocity. In the large diameter column, there is very little effect of slurry flow rate on axial solids distribution; whereas, in the small diameter column, there is a significant effect. At a slurry velocity of 0.02 m/s, the solids concentration profile in both columns is essentially uniform.

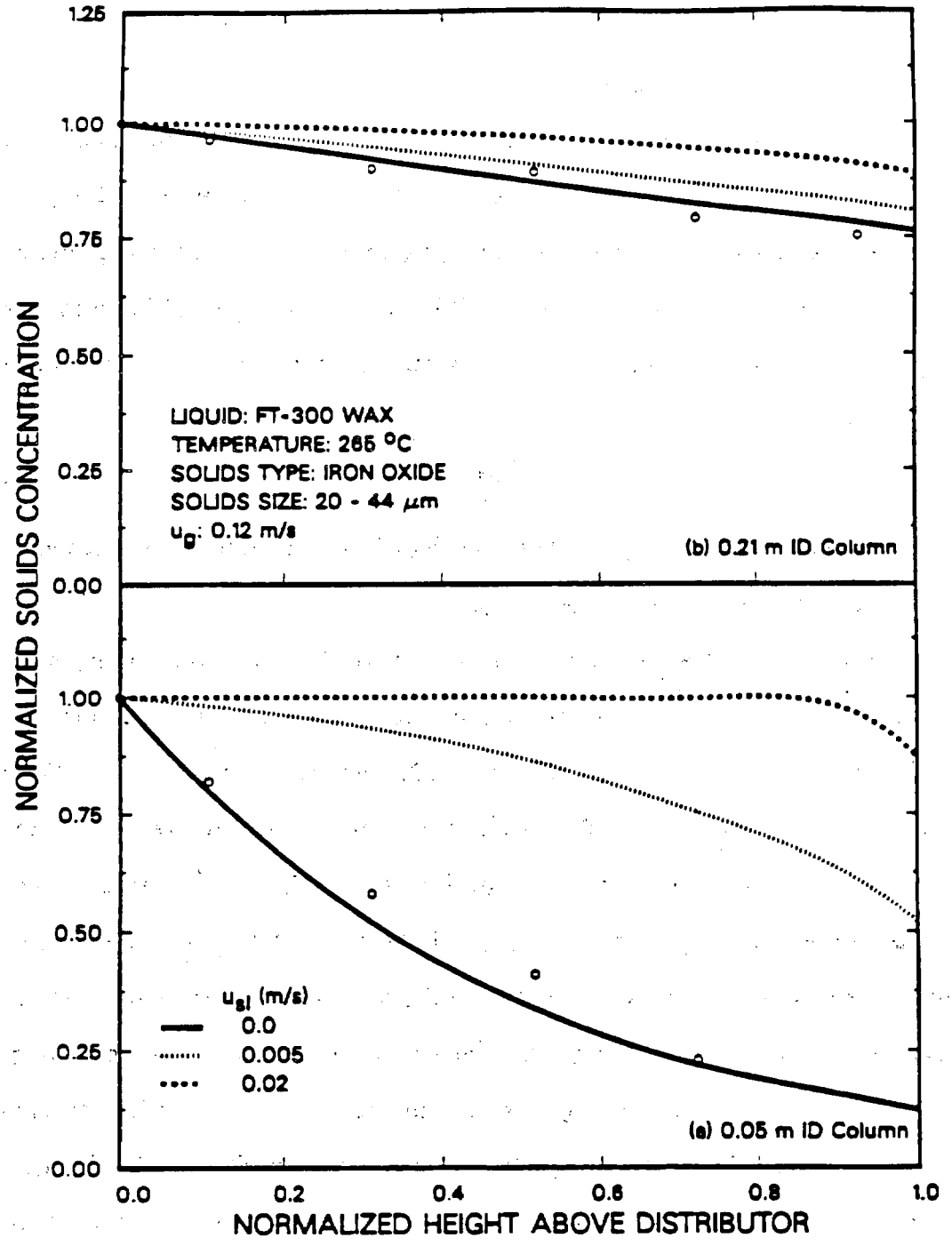

Figure 4.12. Effect of column diameter and superficial slurry velocity on axial solids concentrations.

(○ – Experimental data from batch mode experiments)